Evaluation of seeing-induced cross talk in tip–tilt-corrected solar polarimetry

Philip G. Judge, David F. Elmore, Bruce W. Lites, Christoph U. Keller, and Thomas Rimmele

We reanalyze the effects of atmosphere-induced image motions on the measurement of solar polarized light using a formalism developed by Lites. Our reanalysis is prompted by the advent of adaptive optics (AO) systems that reduce image motion and higher-order aberrations, by the availability of liquid crystals as modulation devices, and by the need to understand how best to design polarimeters for future telescopes such as the Advanced Technology Solar Telescope. In this first attempt to understand the major issues, we analyze the influence of residual image motion (tip–tilt) corrections of operational AO systems on the cross talk between Stokes parameters and present results for several polarization analysis schemes. Higher-order wave-front corrections are left for future research. We also restrict our discussion to the solar photosphere, which limits several important parameters of interest, using some recent magnetoconvection simulations.

OCIS codes: 120.0120, 120.5410.

1. Introduction

Many solar phenomena of current interest are driven by the interaction of turbulent plasma with magnetic fields.[1] Measurements of the full state of polarization of solar spectral lines are needed to infer properties of vector solar magnetic fields from their imprints in the emergent spectra through the Zeeman and Hanle effects.[2] Until the Solar-B satellite[3] is successfully launched, all routine measurements of the solar vector magnetic field must be done from ground-based observatories. All such measurements are detrimentally affected by rapid image distortions introduced by atmospheric seeing, which has significant Fourier power beyond video rates of ≈30 Hz (e.g., see Fig. 1). Even spacecraft measurements are affected to some degree by spacecraft jitter, but, in any case, ground-based polarimetry will remain an important tool for solar physics owing in part to the larger apertures of ground-based telescopes.[4]

Polarized light from astrophysical objects such as the Sun is conveniently described through the Stokes vector $\mathbf{S}$, whose four components S_i, $i = 1, 2, 3, 4$, are usually labeled I, Q, U, and V. In this paper we focus primarily on measuring the magnetic fields in the solar photosphere using the Zeeman effect, and we are concerned with the quiet as well as the active regions of the Sun's atmosphere. In this case all four components of $\mathbf{S}$ are needed to recover the vector magnetic field to within a well-known 180° azimuthal ambiguity. In most cases

$$|I| > |V| > |Q, U|.$$

The order of the inequalities arises because V/I is first order but both Q and U are second order in the ratio of Zeeman splitting to Doppler width, which is often a small parameter. The amplitudes of V, Q, and U are often small compared with I because only a small fraction of the resolution element is occupied by magnetized plasma. Measurements of all four components of $\mathbf{S}$ are generally not made strictly simultaneously. Instead they usually consist of a repeated cycle of sequential measurements through a system (e.g., Fig. 2) designed to modulate, detect, and demodulate the spectral light such that linear combinations of the four components of $\mathbf{S}$ are encoded into time-dependent detector signals, which are proportional to the intensity of the light incident on them. An example of one cycle of a time-dependent modulation and demodulation scheme—the rotating-retarder case studied by Lites[5]—is shown in Fig. 3.

P. G. Judge (judge@ucar.edu), D. F. Elmore (elmore@ucar.edu), and B. W. Lites (lites@ucar.edu) are with the High Altitude Observatory, National Center for Atmospheric Research, P.O. Box 3000, Boulder, Colorado 80307-3000. C. U. Keller (ckeller@nso.edu) and T. Rimmele (rimmele@nso.edu) are with the National Solar Observatory, P.O. Box 26732, Tucson, Arizona 85726.

Received 4 November 2003; revised manuscript received 14 April 2004; accepted 19 April 2004.

0003-6935/04/193817-12$15.00/0

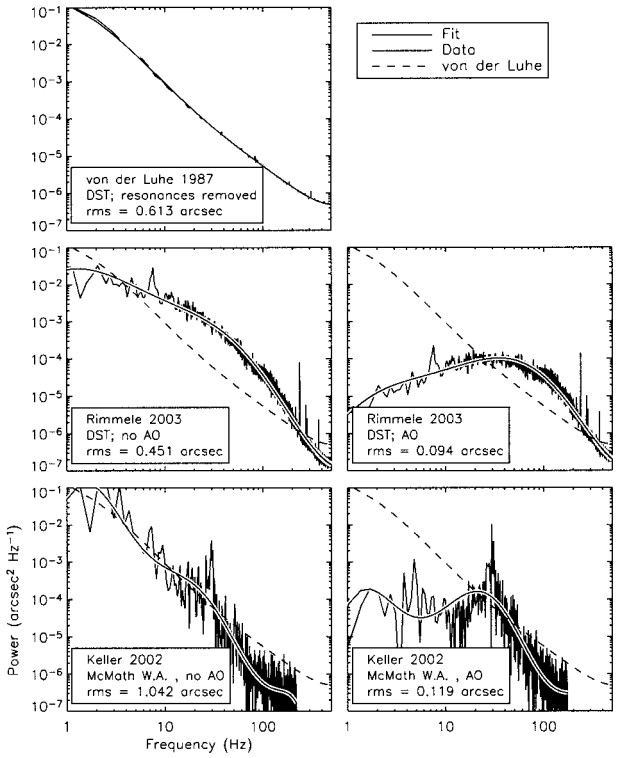

Fig. 1. Power spectra of image motion measured at the Dunn Solar Telescope (DST) at the National Solar Observatory (Sunspot, New Mexico) and at the McMath-Pierce West Auxiliary (W.A.) Telescope on Kitt Peak. The data of von der Luhe were presented by Lites.[5] The other data have not been previously published.

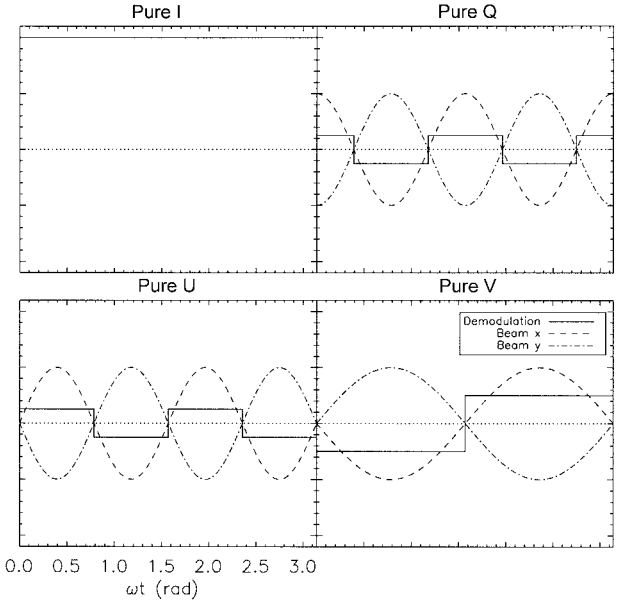

Fig. 3. Example of one cycle of a time-dependent modulation and demodulation scheme—the smoothly rotating retarder case studied by Lites.[5] The abscissa shows the phase angle of the retarder relative to a given reference direction, and the time span plotted shows just one half of a complete rotation of the retarder. The histograms shown correspond to integrations of counts over the time intervals shown, and the sinusoidal curves show the outputs for constant values of (fictitious) pure Stokes parameters Q, U, and V measured at two detectors, x and y. One complete measurement consists of a series of repetitions of such cycles.

The histograms shown correspond to integrations of counts over the time intervals shown. One entire measurement corresponds to an integer number of such cycles. The time-dependent signals are sometimes referred to as modulation states. We can write the measurements using matrices.[6,7] Following del Toro Iniesta and Collados,[7] let $\mathbf{O}$ be the ($n \times 4$) modulation matrix; then the measured signals are

$$\mathbf{I}_M = \mathbf{OS}. \tag{1}$$

There are n elements of the vector $\mathbf{I}_M$, each corresponding to one linear combination ($=I + aQ + bU + cV$) of the input Stokes parameters $\mathbf{S}$ measured over one particular time interval, between say t and $t + \tau$. In the case shown in Fig. 3, for example, $n = 8$ (i.e., eight integrations are needed to extract all four Stokes parameters for the time period plotted). Because the amount of polarization is usually small [i.e., $I > (Q^2 + U^2 + V^2)^{1/2}$], measurements are often made with a dual-beam setup (Fig. 2) in which a beam splitter is used followed by two orthogonal linear polarizers to obtain genuinely simultaneous measurements at two detectors, x and y. The first measures $I_x = I + aQ + bU + cV$, the second measures $I_y = I - aQ - bU - cV$. When combined with reasonably fast polarization modulation, the differences $I_x - I_y$ yield far more accurate values for Q, U, and V than does a single-beam arrangement because the dual-beam approach reduces spurious signals due to seeing-induced variations in Stokes I. However, the difference between the two beams is affected by flat-field errors, which are of the order of 1%. Fortunately, these errors are multiplicative in the polarized Stokes parameters if the main polarization discriminator is a temporal modulation.

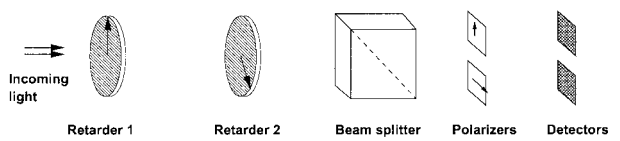

Fig. 2. Schematic optical layout for the modulation schemes considered here. Light from the telescope enters the polarimeter from the left and is registered in the two detectors at the right. In the case of the single rotating-retarder scheme, the second retarder is absent.

The input Stokes vector is recovered from the measured intensities by application of a demodulation matrix $\mathbf{D}$, which can also include necessary algebra for dual-beam systems (made explicit by Seagraves and Elmore[6]):

$$\mathbf{S} = \mathbf{DI}_M = \mathbf{DOS}. \tag{2}$$

To measure all four components of $\mathbf{S}$, $\mathbf{O}$ must be of rank four.[7] If, for each beam, $\mathbf{O}$ is a 4×4 matrix, then $\mathbf{D}$ is unique; but if $n > 4$, an infinite number of demodulation matrices can be used to recover $\mathbf{S}$. del

Toro Iniesta and Collados[7] showed how to compute **D** for a given **O** to minimize the uncertainties in the measurement process represented by Eq. (2) for modulated signals $\mathbf{I}_M$ having statistically the same uncertainty, for example, from photon-counting statistical noise.

The aim of this paper is to study a different source of noise, which is actually a spurious signal introduced by the measurement process. The spurious signals arise from the sequential, nonsimultaneous nature of the measurement process, where time variations of I, Q, U, and V during the exposure period for each measurement $\mathbf{I}_M$ lead to errors in the recovery of **S** by use of Eq. (2). The time variations of most concern here arise from rapid image motions introduced by seeing in the Earth's atmosphere and from slower (but significant when observed at high-angular-resolution) small-scale motions of the solar atmosphere itself. Lites[5] presented a formalism based on Fourier analysis by which the former source of noise—the cross talk between the measured solar Stokes parameters induced by atmospheric seeing—could be easily evaluated. The strength of Lites's analysis lies in the fact that the rms cross talk can be evaluated given just three quantities: the power spectrum of the image motion, the Fourier characteristics of the polarization modulation and demodulation scheme, and the (quasi-static) spatial gradients of Stokes parameters in the solar data. Figure 1 shows some image motion power spectra obtained at the Dunn Solar Telescope (DST) on Sacramento Peak and at the McMath-Pierce West Auxiliary Telescope on Kitt Peak. It also shows, for comparison, the power spectrum obtained by von der Lühe that was used in Lites's original analysis.[5] These are all power spectra of the residual translational motions, including tip–tilt corrections in the case of data collected by Rimmele and Keller. To complete one measurement cycle [i.e., obtain all n components of the vector $\mathbf{I}_M$ in Eq. (2)] requires n measurements for each beam. Lites considered a continuously or stepped rotating retarder, which requires $n \geq 6$ for measurement of the full Stokes vector **S**, and both single- and dual-beam systems. For a read rate of f_R hertz, each complete measurement requires at least Kn/f_R seconds, where K is the number of repetitions of the measurement cycle. At video frame rates ($f_R \approx 30$ Hz), all image motion power spectra have significant power beyond the 5-Hz cadence implied when $n = 6$ (Fig. 1). Thus seeing-induced noise remains an issue for these schemes.

Since Lites's research, several technological advances have occurred, prompting us to reinvestigate the issue of polarization cross talk. The first advance concerns the ability of detectors to demodulate at frequencies of tens of kilohertz, i.e., much higher than those where the bulk of the seeing exists. As noted by Keller,[8] in 1969 Kemp suggested that photoelastic modulators could in principle be used to beat or freeze essentially all the seeing-induced image motion if the modulated signals could be demodulated. Stenflo and Povel[9] proposed use of a novel kind of optical demodulation device. Such modulators and detector devices have since been realized and have yielded high-sensitivity polarization measurements made at visible wavelengths[10,11] and offer an important solution to the problems introduced by atmospheric seeing. These devices have historically had the problem of a low efficiency associated with the required masks needed for charge storage areas on the detector and the restriction of a single CCD demodulator to one frequency. Solutions to these problems have not yet been fully overcome (Keller[8] discusses these and other issues). We do not discuss these devices further because they do not suffer from the effects investigated here.

The second advance involves the introduction of adaptive optics (AO) as a way to reduce the detrimental effects of seeing on the polarization measurements. If we restrict our discussion simply to residual image motion (i.e., tip–tilt corrections), ignoring the higher-order AO corrections (astigmatism, defocus, coma), we can expect that an effective AO system will significantly reduce the polarization cross talk because it depends linearly on the rms image motion[5] [see Eq. (9)].

Assuming, for the sake of simplicity that turbulence in the Earth's atmosphere obeys a Kolmogorov spectrum, after complete tip–tilt correction the total variance of the wave-front errors in radians squared reduces from $1.03(D/r_0)^{5/3}$ to $0.134(D/r_0)^{5/3}$, where D is the telescope aperture and r_0 is Fried's seeing parameter (e.g., Roddier[12]). Of course no AO system completely eliminates image motion. For example, our tip–tilt-corrected spectra are influenced by telescope shake and instrument jitter, which are clearly not Kolmogorov in terms of their power spectrum. Thus we always need to consider the temporal power spectrum of the remaining image motion (Fig. 1), and it is important to understand the influence of this effect on the cross talk.

A third advance involves the more common use of liquid-crystal devices for polarization modulation. Ferroelectric liquid crystals (FLCs) and liquid-crystal variable retarders (LCVRs) have some advantages over the early rotating-retarder schemes analyzed by Lites, in that modulation and demodulation schemes can be constructed to optimize the efficiency of the analysis[7] and to give equal weight to all three polarized Stokes parameters Q, U, and V for every single modulation state (balanced modulation).

For these reasons, we have undertaken a study of the effects of image motion-induced cross talk including the effects of AO image correction and different polarization analysis schemes that take advantage of several different modulation devices. We also examine the spatial properties of the Stokes vectors predicted from recent magnetoconvection simulations to translate the computed values of the rms cross talk into signal-to-noise ratio estimates of the derived Stokes parameters. We conclude with a discussion of implications for existing and new ground-based instrumentation, including the new Swedish Solar

Telescope[13] and the future Advanced Technology Solar Telescope[4] (ATST).

2. Formalism

Our formalism follows that of Lites.[5] Briefly, the light entering a polarimeter is described by the Stokes vector $\mathbf{S}(x, y; t)$, where x, y describe coordinates in the position on the plane of the sky and t is time. In a seeing-free situation

$$S_i(x, y; t) = R_i(x, y; t), \tag{3}$$

where $R_i(x, y; t)$ is the Stokes vector unaffected by seeing. When seeing-induced image motion is present, neglecting higher-order image aberrations, the input Stokes vector at instant t corresponds to that from a position x', y':

$$S_i(x, y; t) = R_i(x', y'; t). \tag{4}$$

For small deviations we can write

$$S_i(x, y; t) \approx R_i(x, y; t) + \nabla R_i(x, y; t) \cdot \mathbf{s}(t), \tag{5}$$

where $\mathbf{s}(t) = (x' - x, y' - y)^T$ is the seeing-induced image displacement at time t. $\mathbf{s}(t)$, driven by atmospheric turbulence, has no preferred direction when averaged over time, so we can replace the dot product in approximation (5) with the angle-averaged value $|\overline{\nabla R_i}|$, multiplied by the scalar quantity $\sigma N(t)$, where σ is the rms value of the seeing and $N(t)$ describes the seeing function with zero mean and unit rms. Note that, if the image motion power spectra are measured relative to just one axis (i.e., tip or tilt), the power spectra should be multiplied by a factor of 2—i.e., σ should be multiplied by $\sqrt{2}$—to account for the additional variations along the orthogonal axis. Dropping the coordinates $(x, y; t)$, we obtain

$$S_i \approx R_i\left[1 + \frac{\overline{|\nabla R_i|}}{|R_i|}\sigma N(t)\right], \tag{6}$$

$$= R_i[1 + \beta_i N(t)], \tag{7}$$

which is Eq. (1) of Lites,[5] taking into account his Eq. (3). We define $P_N(\nu)$ as the normalized power spectrum of $N(t)$, where[5]

$$\int_0^\infty P_N(\nu)\mathrm{d}\nu = 1. \tag{8}$$

Lites[5] envisaged a polarization analysis system consisting of just a single rotating retarder whose fast axis varies with time either continuously or in a stepped fashion, followed by a beam splitter that separates the emergent modulated light into orthogonal states of polarization onto two different detectors (see Fig. 2; in this particular case one of the retarders is absent and the other rotates in time). Calculation of the modulated and demodulated signals as a function of time onto the two detectors and subtraction of the signals of the two detectors yields, after some algebra, the following expression[5] for the rms cross talk from Stokes parameter i to Stokes parameter r:

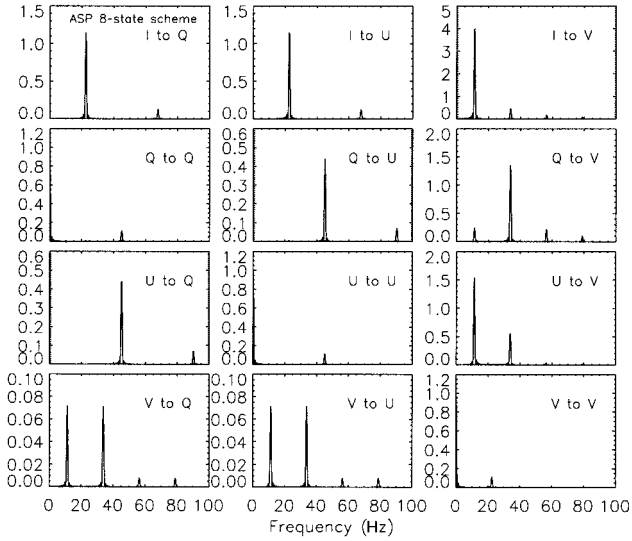

Fig. 4. Polarimeter cross-talk response matrices $[|\tilde{H}_{ri}'(\nu)|^2]$ plotted as a function of frequency for the continuously rotating retarder used in the Advanced Stokes Polarimeter (ASP). The total integration time is 1 s, and the read time is 0.11 s.

$$\sigma_{ri}^{\,2} = (R_i\beta_i)^2 \int_0^\infty |\tilde{H}_{ri}'(\nu)|^2 P_N(\nu)\mathrm{d}\nu, \tag{9}$$

where $\tilde{H}_{ri}'(\nu)$ is the Fourier transform of the product of the modulation function for the input of parameter i with the demodulation function for parameter r. Equation (9) shows that $|\tilde{H}_{ri}'(\nu)|$ should be viewed as a polarimeter response matrix for the cross talk (off-diagonal elements) and noise (diagonal elements) as a function of frequency. Figures 4 and 5 show several frequency-dependent examples of these matrices for the case of a continuously rotating retarder and the double LCVR-balanced modulation and demodulation scheme of Sánchez Almeida[14] (see Subsections 2.A and 2.B and Table 1). These can be compared with Fig. 1. These matrices have the following general properties:

1. They are strongly peaked at frequencies that are harmonics of $\mathcal{T}^{-1}$, where $\mathcal{T}$ is the time for a full modulation or demodulation cycle (such as the one shown in Fig. 3).
2. Thus, with smaller $\mathcal{T}$, the contributions to the cross talk and noise arise from higher frequencies, sampling different values of $P_N(\nu)$.
3. They strongly depend on the type of modulation scheme and the particular Stokes parameters being computed.
4. For a fixed modulation rate but varying total exposure times, the widths of the peaks and their accompanying sidebands decrease linearly with total exposure time, but the maxima remain unchanged. Thus the rms cross talk depends on the square root of the total exposure time [Eq. (9)].

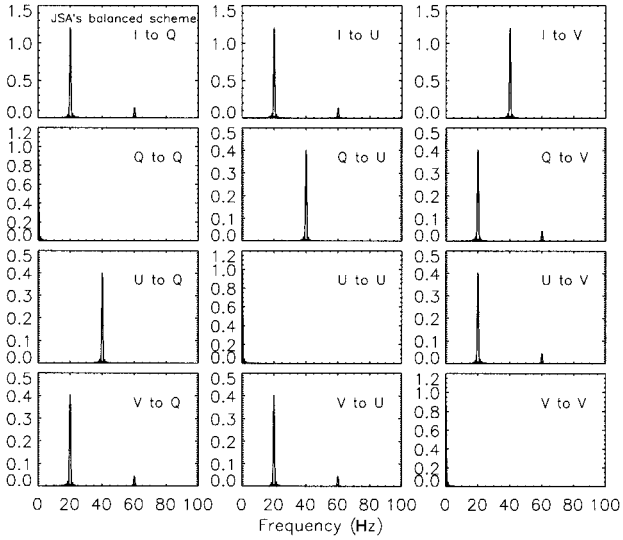

Fig. 5. Polarimeter cross-talk response matrices $[|\tilde{H}_{ri}'(\nu)|^2]$ plotted as a function of frequency for the balanced scheme of Sánchez Almeida (JSA) (see Table 1). The total integration time is 1 s, and the read time is 0.11 s.

5. For a fixed total exposure time but with varying cycle times $\mathcal{T}$, the functions $\tilde{H}_{ri}'(\nu)$ have the same form but they simply shift in frequency linearly with $\mathcal{T}^{-1}$, such that $\int_0^\infty |\tilde{H}_{ri}'(\nu)|^2 d\nu$ = constant. Thus the magnitude of the cross talk varies with $\mathcal{T}$ for a fixed total exposure time only through the shape of the product of $|\tilde{H}_{ri}'(\nu)|^2$ and $P_N(\nu)$ [Eq. (9) again].

Below we envisage other types of polarization modulation systems, in which LCVRs and FLCs replace the rotating-retarder system, but the beam-splitting arrangement remains the same. We can also use Lites's formalism[5] for these schemes and Eq. (9) with appropriately modified expressions for $\tilde{H}_{ri}'(\nu)$. For this reason it is important to recall the assumptions that underlie it:

1. Time dependence arises solely from seeing-induced image motion noise, not solar evolution; and

2. the noise is stationary [statistically, $\langle N(t)\rangle = \langle N(t + \tau)\rangle$] when averaged over typical integration times.

A. Rotating Retarders

Rotating retarders will probably remain an important component of solar Stokes polarimetry for some time in spite of the newer modulation devices because the latter have several physical limitations (e.g., the photon fluxes incident on them are limited; the physical size of some devices is also limited; times for changing polarization states are significant, being $\approx$17 ms for the devices considered by Sánchez Almeida[14]). Furthermore, rotating retarders can handle polarimetry over a broad range of wavelengths simultaneously by use of low-order retarders with the various orders being matched to the wavelengths of interest or through use of an achromatic retarder over a narrower wavelength range.

Lites's formalism[5] and notation for rotating retarders is adopted here. In Appendix A we provide corrections for some typographical errors in Lites's original paper, uncovered during the course of the present work.

B. Other Modulation and Demodulation Schemes

The advent of FLCs and LCVRs has led to new modulation and demodulation schemes that differ significantly from those achievable with rotating retarders. In particular, combinations of these newer devices can produce so-called balanced schemes in which equal weight is given to the measurement of the Q, U, and V parameters during the modulation and demodulation cycles. Unlike rotating retarders, in which V is always modulated at one half of the frequency of Q and U, the relative modulation frequencies can to some degree be chosen. For example, the double LCVR-balanced scheme of Sánchez Almeida[14] modulates V at twice the frequency of Q and U. Furthermore, these schemes yield signals without the dc component present in Q in all rotating wave plates whose retardance δ yields nonzero modulation of V (see Lites's[5] Table I). We consider schemes that approach 100% efficiency in the sense defined by del

Table 1. Examples of Polarimeter Setups Examined Here[a]

Scheme	Retarder 1		Retarder 2		Examples and References
	δ_1[b]	θ_1[b]	δ_2	θ_2	
1. Single rotating retarder	Fixed	Rotating			ASP[c]
2. Single rotating retarder	Fixed	Stepped			Lites[d]
3. Two LCVRs	Stepped	Fixed	Stepped	Fixed	SST[e]
4. Two FLCs	Fixed	Stepped	Fixed	Stepped	TIP,[f] SOLIS,[g] DLSP[h]

[a]Refer to Fig. 2 for the schematic layout of the retarders in the polarimeters envisaged here.
[b]δ and θ refer to retardances and angles of the fast axes of the retarders, respectively.
[c]Ref. 15.
[d]Ref. 5.
[e]SST, Swedish Solar Telescope.[14] This scheme was devised by Jorge Sanchéz Almeida (JSA).
[f]TIP, Tenerife Infrared Polarimeter.[16]
[g]SOLIS, Synoptic Optical Long-Term Investigations of the Sun.[17]
[h]Ref. 18.

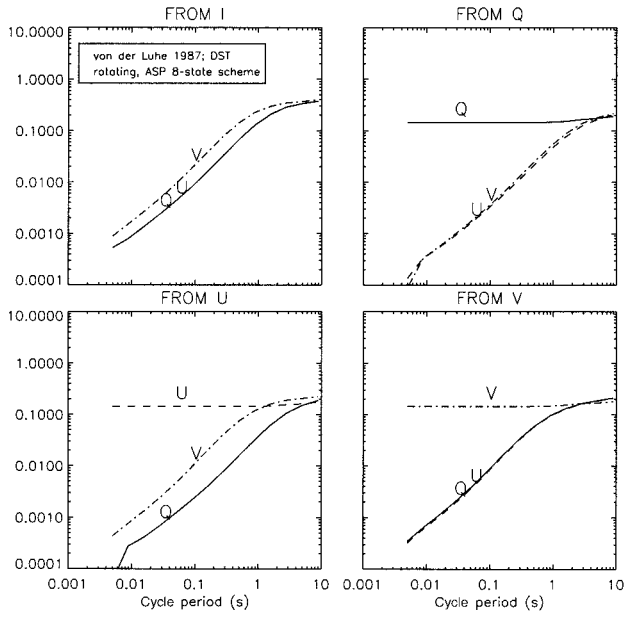

Fig. 6. Normalized cross-talk values C_{ri} [Eq. (10)] as a function of cycle period for the ASP (single rotating retarder) with von der Lühe's (see Lites[5]) residual image motion power spectrum. An integration time of 10 s was assumed. The format of the plot follows Lites,[5] except that the abscissa values are half of those plotted by Lites.

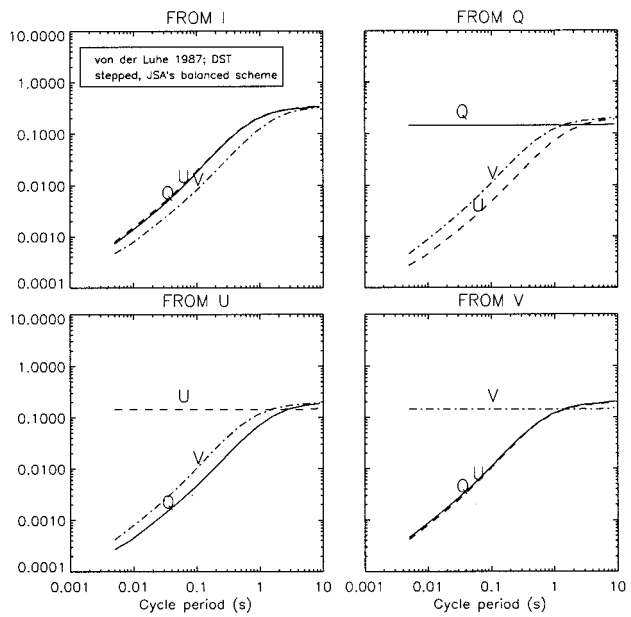

Fig. 7. Normalized cross-talk values C_{ri} [Eq. (10)] as a function of cycle period for the modulation scheme of Sánchez Almeida (JSA) (two LCVRs) by use of von der Lühe's (see Lites[5]) residual image motion power spectrum. An integration time of 10 s was assumed.

Toro Iniesta and Collados.[7] The modulation and demodulation matrices are combined to optimize the polarimetric efficiency. We also consider schemes that are balanced.

Figure 2 shows the measurement setup envisaged for the modulation schemes we discuss here, and Table 1 summarizes the type of devices used in existing schemes. In some schemes, modulation is performed by means of rapidly changing the states of the retarder(s), and the counts are recorded at the detectors while the retarders are held in each fixed state for a time τ. The Advanced Stokes Polarimeter (ASP) and other polarimeters accumulate counts while the retarder rotates at a fixed angular velocity. Demodulation is performed by means of assembling the count rates into the vector $\mathbf{I}_M$ and applying the demodulation matrix [Eq. (2)].

3. Results

A. Comparing Single Rotating Retarders with Other Schemes

Before studying the dependence of cross talk on adaptive optical correction of image motion, it is interesting first to compare a rotating single retarder—such as that used in the ASP[15]—with liquid-crystal devices that combine two retarders. Figure 6 shows the magnitude of the cross talk computed for the single-retarder ASP modulation and demodulation scheme. Figure 7 shows cross talk computed with the double LCVR-balanced scheme of Sánchez Almeida.[14] Figures 6 and 7 follow the form shown by Lites,[5] except that the abscissa shows the time taken to perform one entire measurement cycle, i.e., one half of the rotation of the wave plate for the single rotating retarder (Lites's figures show on the abscissa the time needed for a complete rotation of the wave plate) or one complete set of states for the LCVR case. The ordinates show the quantity

$$C_{ri} = \left[\int_0^\infty |\tilde{H}_{ri}'(\nu)|^2 P_N(\nu) \mathrm{d}\nu \right]^{1/2}$$

so that the actual cross talk from Stokes parameter i to parameter r is, from Eq. (9),

$$\sigma_{ri} = R_i' \beta_i C_{ri}, \tag{10}$$

where $R_i' = R_i$ for $i = 1 \ldots 4$ if just a single beam is measured. Results are shown for total integration times of 10 s, which is close to the upper limit imposed because of the evolution of small magnetic features in the solar photosphere, as observed at the resolution limit of the ATST (see Keller[19] and below). When dual beams are measured, R_1' is instead the detector imbalance term.[5] In this case, $R_1' = (\Delta_x - \Delta_y)/2$, where $\Delta_\alpha = (\gamma_\alpha/\Gamma_\alpha) - 1$ for each detector $\alpha = x$ or y; here γ_α is the (actual, but unknown) factor relating count rates on detector α to the intensity incident on the detector, and Γ_α is the known value of γ_α determined through calibration. For any reasonable polarimeter, it can be assumed that the calibration is known to better than a few percent, i.e., $|\Delta_\alpha| \ll 1$.

Figures 6 and 7 show a monotonic decline of cross talk with decreasing cycle period, reflecting the monotonic decrease of the image motion power spec-

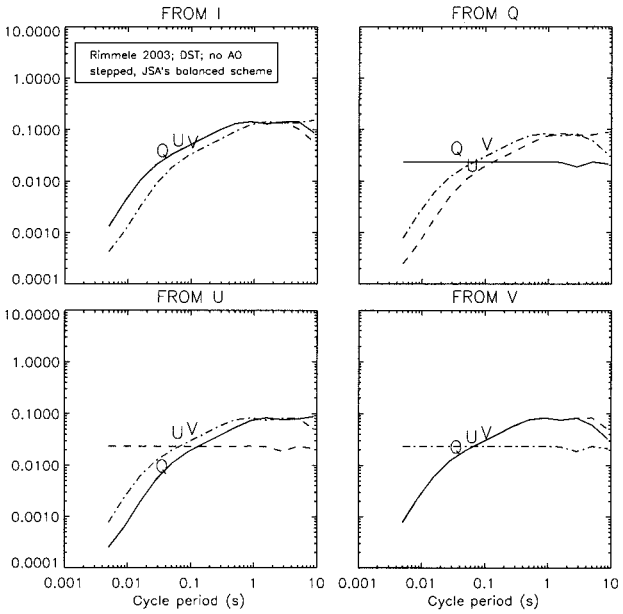

Fig. 8. Normalized cross-talk values C_{ri} [Eq. (10)] as a function of cycle period for Sánchez Almeida's (JSA's) double LCVR measurement scheme by use of the nontip–tilt-corrected image motion power spectrum measured by Rimmele at the DST. An integration time of 10 s was assumed.

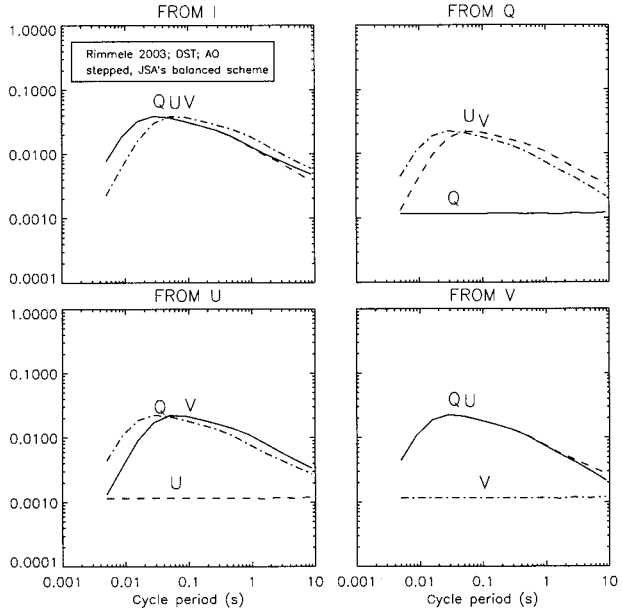

Fig. 9. Same as Fig. 8 except that the tip–tilt-corrected image motion power spectrum measured by Rimmele at the DST was used. JSA, J. Sánchez Almeida.

trum with frequency. Comparison of Figs. 6 and 7 shows that the cross talk differs by up to a factor of 3 between these particular schemes for a given cycle period. The diagonal components C_{rr} are larger for the ASP rotating retarder because of the continuously varying retarder fast-axis orientation during the integrations, which leads to a lower average signal (the transmitted signals of pure Q, U, or V go smoothly to zero at the beginning and end of each integration period—see Fig. 3). The off-diagonal cross talk for the ASP $I \rightarrow QU$ is similar to the $I \rightarrow V$ cross talk for the LCVR scheme, and vice versa. The $V \rightarrow QU$ cross talk is similar for the two schemes. The $Q \rightarrow U$ cross talk is also almost identical for the two schemes, but the ASP $U \rightarrow Q$ cross talk is a factor of 2 lower for the ASP scheme compared with the LCVR scheme. The cross talk from QU to V is, under ideal conditions, negligible in the weak-field limit of the Zeeman effect. However, when systematic errors (due, for example, to finite telescope polarization because of nonnormal incidence reflections[19]) are present, such cross talk is an issue. The $Q \rightarrow V$ cross talk is a factor of 3 larger for the LCVR scheme than for the ASP scheme. A similar figure with the FLC scheme[16] developed at the Instituto Astrofisico Canarías shows similar results, but, because that scheme gives greater weight to the measurement of V over each cycle, the cross-talk terms for $Q, U \rightarrow V$ are smaller, and $Q \rightarrow U$, $U \rightarrow Q$ are larger by factors of 2 to 3.

B. Effects of Tip–Tilt Corrections on Cross Talk

Figures 8 and 9 show cross-talk calculations for the double LCVR-balanced scheme of Sánchez Almeida[14] for residual image motion power spectra that are uncorrected and corrected by use of the current (i.e., just tip–tilt) National Solar Observatory (NSO) AO system, respectively. Both systems can also correct higher-order aberrations, but the corresponding analysis is beyond the scope of this paper. The power spectra correspond to a rms image motion of 0.45 and 0.09 arcsec, respectively. Figure 8 is qualitatively similar to Fig. 7, showing an almost monotonic decline of cross talk with decreasing cycle period. Figure 9 is quite different: There is a resonance between the broad residual power spectrum peak near 40 Hz and the peaks in the polarimeter cross-talk response matrices ($|\tilde{H}_{ri}'(\nu)|^2$), leading to a broad maximum in the off-diagonal cross-talk values near cycle periods of 0.05 s (20 Hz, read times of 0.0125 s, a read frequency of 80 Hz). We note that 40 Hz is twice $\mathcal{T}^{-1}$. These cross-talk values decline sharply as $\mathcal{T}$ is decreased from its value near the cross-talk maxima, roughly as $\mathcal{T}^{-1}$, and less sharply as $\mathcal{T}^{-1/2}$ when $\mathcal{T}$ is increased. Similar results are found for the FLC scheme developed at the Instituto Astrofisico Canarias. It is important to stress that, in spite of this resonance, the smaller integrated power in the tip–tilt-corrected data (as measured by the rms seeing) leads to cross-talk values that are always smaller than those for the nontip–tilt-corrected data.

Results for the new Synoptic Optical Long-Term Investigations of the Sun (SOLIS) vector spectromagnetograph system[17] (a double FLC scheme, results not shown, also used by the diffraction-limited spectropolarimeter) are quite similar to those shown in Figs. 8 and 9. However, the $IUV \rightarrow Q$ cross talk is a factor of 2 to 3 lower, and the $Q \rightarrow UV$ cross talk is some 50% higher. This difference results from the

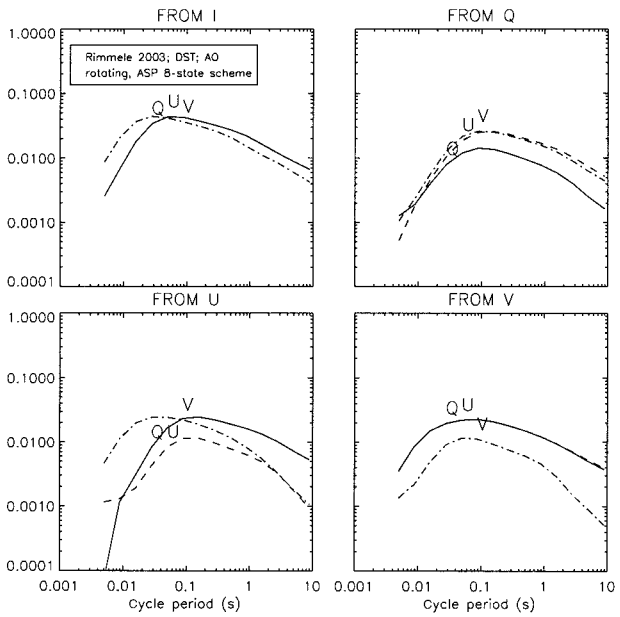

Fig. 10. Same as Fig. 9 except that the rotating retarder and ASP demodulation scheme were used.

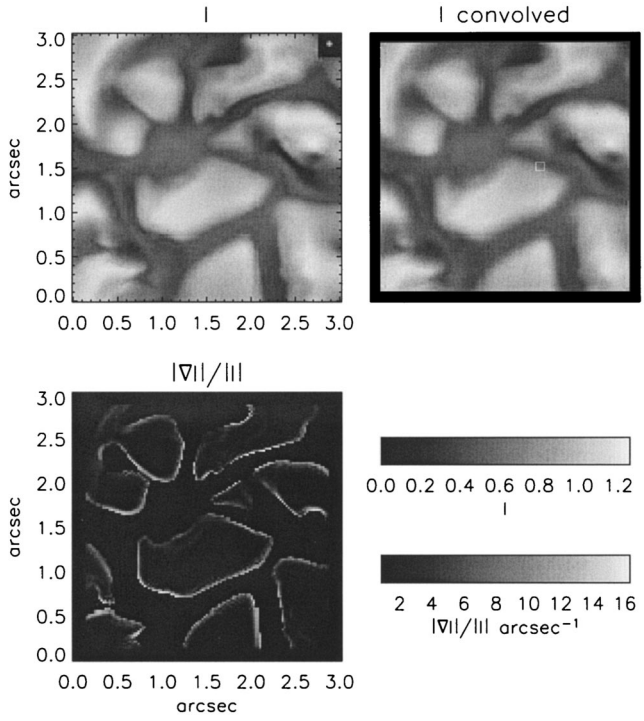

Fig. 11. Computed intensities I from the magnetoconvection simulation, modeled for a typical region of the quiet Sun. The raw data (top left) were convolved (top right) with a Gaussian function representative of the resolution limit of the ATST. The lower left panel shows $|\nabla I|/|I|$ computed from the convolved image. The region enclosed in a white box shows a representative strong internetwork magnetic field element whose signal-to-noise ratio properties are estimated in Table 2.

higher weight given to measurements of Q during the modulation and demodulation cycle in the SOLIS scheme.

The results differ when a continuously rotating retarder is used, especially for the diagonal elements (compare Fig. 10 with Fig. 9). The diagonal components of the matrices $|\hat{H}_{rr'}(\nu)|^2$ for continuously rotating retarders have significant secondary maxima away from the primary maxima that are at zero frequency (Fig. 4). The secondary peaks arise from the fact that the polarization states vary during the integrations (see Fig. 3), yielding power at frequencies that are multiples of $\mathcal{T}^{-1}$, which lead to the frequency dependence shown in Fig. 10. Secondary peaks are absent in the equivalent matrices for other schemes whose polarization states are fixed during the integrations.

C. Case Study: Cross Talk in Synthetic Quiet Sun Magnetic Fields

To estimate cross talk we need values of $\beta_i = |\nabla R_i|/|R_i|$ [see Eq. (6)]. A major goal of the ATST project—which will use a 4-m telescope—is to measure magnetic structures at the highest possible angular resolution. Until such data become available, we cannot estimate values of β_i from data because the most highly resolved images of the Sun obtained with the new Swedish Solar Telescope are still limited by the diffraction of this 1-m telescope.[20] It is a Catch-22 situation: To estimate the cross talk we must have the data, and to have the best quality data, we must estimate cross talk and take measures to optimize the way that polarimetry is done. Until ideal observations become available, we must therefore rely on simulations. To this end, we used magnetoconvection simulations of Stein and Nordlund,[21] which represent state-of-the-art time-dependent three-dimensional simulations of the magnetized solar photosphere. We simulated the emerging Stokes profiles and examined these simulated observations for both spatial gradients and their time variation. In the simulations, the magnetic field is highly intermittent in space with concentrations confined largely to intergranular lanes and with a rms magnitude of the vertical component of the magnetic field vector of 55 G. In some localized areas the magnetic field strength is well above 1000 G.

1. *Results for a Snapshot from a Simulation*

We now discuss two figures pertaining to one wavelength corresponding to a typical maximum of the Stokes $|V|$ profile for the longer wavelength of the two iron lines at 6302 Å. Figures 11 and 12 show gradients for Stokes I and V, respectively, computed from data (upper right panels) that were convolved with a two-dimensional Gaussian function with a FWHM of 0.0325 arcsec. This corresponds roughly to the point-spread function expected for the ATST at 6300 Å. Note the small physical scale of Figs. 11 and 12. Figure 11 shows that values of $|\nabla I|/|I|$ are limited to values below 15 arcsec^{-1}. In contrast, the Stokes Q, U (not shown), and V parameters show $|\nabla S_i|/|S_i|$ values that approach 100 arcsec^{-1}. This is

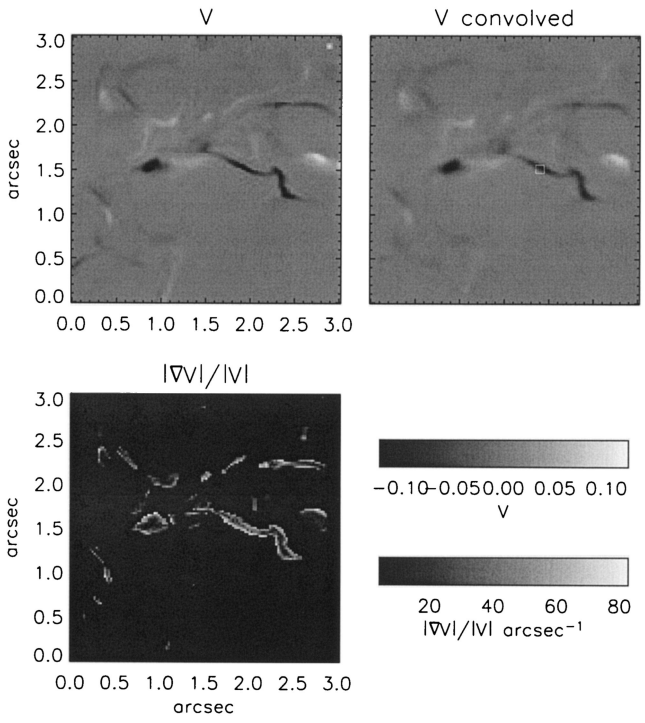

Fig. 12. Same as Fig. 12 except that data are shown for Stokes V. The same figures for Q and U are similar to those modeled for a typical region of the quiet Sun.

easy to understand because I is dominated by thermodynamics, but Q, U, and V are also controlled by magnetic fields, which are not only the desired object for detailed observation but are also highly spatially structured.

With Figs. 11 and 12 we now have all the data needed to assemble the cross talk and obtain the signal-to-noise ratios for some typical measurements, assuming that the synthetic data are representative of what will actually be measured in the quiet Sun. In Figs. 11 and 12 we marked with a box a region containing a strong internetwork magnetic field for closer examination. In Table 2 we list contributions to the cross talk evaluated for this region. The calculations assume a 10-s integration and a 40-Hz read rate, and the $I \rightarrow Q, U, V$ cross talk is set by a beam imbalance of 1%. This beam imbalance is a reasonable estimate given that CCDs might accumulate several million electrons (see Subsection 3.C.2) leading to 0.1% photon noise (a lower limit) and that variations in gain will contribute to the noise systematically. In addition, there may be significant pixel-to-pixel registration mismatches between the two beams leading to additional errors in the balance between the two beams. With these parameters, inspection of Table 2 shows that the tip–tilt system improves the signal-to-noise ratios by a factor close to 10, in spite of the resonance between residual power spectra and the modulation scheme power spectra noted above. With tip–tilt correction, signal-to-noise ratios as high as 30 might be expected, for Stokes V, given these parameters.

Without tip–tilt correction, the signal-to-noise ratios are roughly a factor of 10 smaller. Interestingly, the ASP single rotating-retarder scheme is not dramatically worse than the balanced scheme of Sánchez Almeida—at worst the rotating retarder has signal-to-noise ratios of a factor of 3–4 smaller, at best just 8% smaller. With the parameters used, the cross talk to Q, U, V is dominated by cross talk from $V \rightarrow QU$ or $I \rightarrow QU$ because of the small values of Q and U. Again, we note that $QU \rightarrow QUV$ cross talk may be a significant issue when telescope polarization is taken into account.

2. *Photon Noise*

Under most conceivable conditions in which observations of the Sun's disk will be performed, the photon noise is much smaller than the cross talk evaluated above. If the Sun is imaged with pixels that critically sample the angular resolution of a given tele-

Table 2. Cross-Talk Values $\{R_i\beta_i[\int_0^\infty |\tilde{H}_{ri}'(\nu)|^2 P_N(\nu)\mathrm{d}\nu]^{1/2}\}$ and Signal-to-Noise Ratios for a Typical Magnetic Element[a]

To	From I	From Q	From U	From V	Signal-to-Noise Ratio
JSA's[b] scheme, Rimmele *et al.*[4] spectrum, no AO, $\sqrt{2}\sigma = 6.36(-1)$					
$Q = -3.8(-4)$	1.7(−3)	−5.9(−3)	1.7(−3)	−5.8(−2)	6.5(−3)
$U = 2.9(-3)$	1.7(−3)	−4.3(−3)	2.8(−3)	−5.8(−2)	5.0(−2)
$V = -4.3(-2)$	1.0(−3)	−7.1(−3)	3.7(−3)	−3.6(−2)	1.2(0)
JSA's[b] scheme, Rimmele *et al.*[4] spectrum, AO, $\sqrt{2}\sigma = 1.27(-1)$					
$Q = -3.8(-4)$	2.7(−4)	−5.7(−5)	4.4(−4)	−6.0(−3)	6.4(−2)
$U = 2.9(-3)$	2.7(−4)	−8.5(−4)	2.9(−5)	−6.0(−3)	4.8(−1)
$V = -4.3(-2)$	2.7(−4)	−1.2(−3)	6.1(−4)	−4.0(−4)	3.0(1)
ASP 8-state scheme, Rimmele *et al.*[4] spectrum, AO, $\sqrt{2}\sigma = 1.27(-1)$					
$Q = -3.8(-4)$	2.4(−4)	−6.6(−4)	4.9(−4)	−6.6(−3)	5.7(−2)
$U = 2.9(-3)$	2.4(−3)	−1.3(−3)	2.4(−4)	−6.6(−3)	4.0(−1)
$V = -4.3(-2)$	2.7(−4)	−1.4(−3)	5.4(−4)	−3.3(−3)	1.2(1)

[a] $x, y(z) \equiv x, y \times 10^z$. All entries are for a 10-s integration and a 40-Hz read rate. In these calculations we assume that the $I \rightarrow Q, U, V$ cross talk is set by a beam imbalance of 1% (see text). The values of I, Q, U, and V that we used were extracted from the boxed regions in Figs. 11 and 12. The units are such that values of I are near unity.

[b] J. Sánchez Almeida.[14]

scope, the projected angular size of the pixels must be $px_{\mathrm{DL}} = \lambda/2D$, where λ is the wavelength and D is the telescope aperture. The number of photons ${N_{\mathrm{DL}}}^{\mathrm{photons}}$ accumulated in a pixel of this projected angular size in t seconds is

$$ {N_{\mathrm{DL}}}^{\mathrm{photons}} = E[B_{\lambda}(T)\mathrm{d}\lambda]\omega_{\mathrm{DL}} t \frac{\pi}{4} D^2, \tag{11} $$

$$ = \frac{\pi}{16} E[B_{\lambda}(T)\mathrm{d}\lambda]\lambda^2 t, \tag{12} $$

where E is the overall system efficiency, $B_{\lambda}(T)$ is the Planck function at temperature T and wavelength λ, $\mathrm{d}\lambda$ is the spectral bandpass, and $\omega_{\mathrm{DL}} = {px_{\mathrm{DL}}}^2$. When observed at a fixed value of λ/D, such as at the diffraction limit, Eq. (12) shows that this signal-to-noise ratio is independent of telescope aperture D. Using parameters for the 6302-Å lines observed with the D = 4-m-diameter ATST, in the general case where the pixel size px is not necessarily equal to px_{DL} = 0.0162 arc sec, we obtain

$$ N^{\mathrm{photons}} = 1.1 \times 10^7 \frac{E}{0.05} B_{6302\text{Å}}\left(\frac{T}{5000\ \mathrm{K}}\right) \frac{\mathrm{d}\lambda}{22\ \mathrm{mÅ}} \times \left(\frac{px\ \mathrm{arcsec}}{0.0162}\right)^2 \left(\frac{D}{400\ \mathrm{cm}}\right)^2 \frac{t}{10\ \mathrm{s}}. \tag{13} $$

When $px = px_{\mathrm{DL}}$, this yields a signal-to-noise ratio $I/\sigma(I) = (N^{\mathrm{photons}})^{1/2} = 3 \times 10^3$ from photon-counting statistics alone. Because the measurements of Q, U, and V are always made in linear combination with I, and because $|I| > |V| > |Q, U|$, the signal-to-noise ratios for V (and similarly for Q, U) are $\approx V/\sigma(I)$. In the magnetic element studied in Table 2, $|V| \approx 0.043|I|$, so that $V/\sigma(I) \approx 47$. The equivalent numbers for the much smaller values of Q and U from the table yield $Q/\sigma(I) \approx 0.4$ and $U/\sigma(I) \approx 3$, both an order of magnitude larger than the tip–tilt-corrected cross-talk values listed in Table 2. It is unlikely that spectropolarimetry at facilities like the ATST will be done at the diffraction limit, so that the signal-to-photon-noise ratios will be even higher than this estimate. Even in the diffraction-limited case, the photon noise is somewhat less than the cross-talk values and will be correspondingly smaller when observations are made with pixel sizes larger than the diffraction-limited size.

3. *Exposure Time Limits Set by Solar Evolution*

Figures 11 and 12 are for one snapshot of a dynamic simulation. Two images computed 30 s before and after these data were used to determine time derivatives. Figures 13 and 14 show the time derivatives $|\mathrm{d}S_i/\mathrm{d}t|$ and the time scales $|S_i/(\mathrm{d}S_i/\mathrm{d}t)|$ from the convolved images. Again, results (not shown) for Q and U are similar to those for V, and yet again the derivatives for I are small and those for Q, U, and V are nearly an order of magnitude larger for the same reasons given above. Figures 13 and 14 illustrate that, in regions of strong magnetic field [indicated in these data by large values of $(Q^2 + U^2 + V^2)^{1/2} \approx V$], the features evolve on time scales whose mode in the distributions is near 30 s. In other words, if 30-s integrations were used to accumulate data, the features would have changed by a factor of e. Stokes parameter S_i changes from ${S_i}^0$ in time δt due to solar evolution as

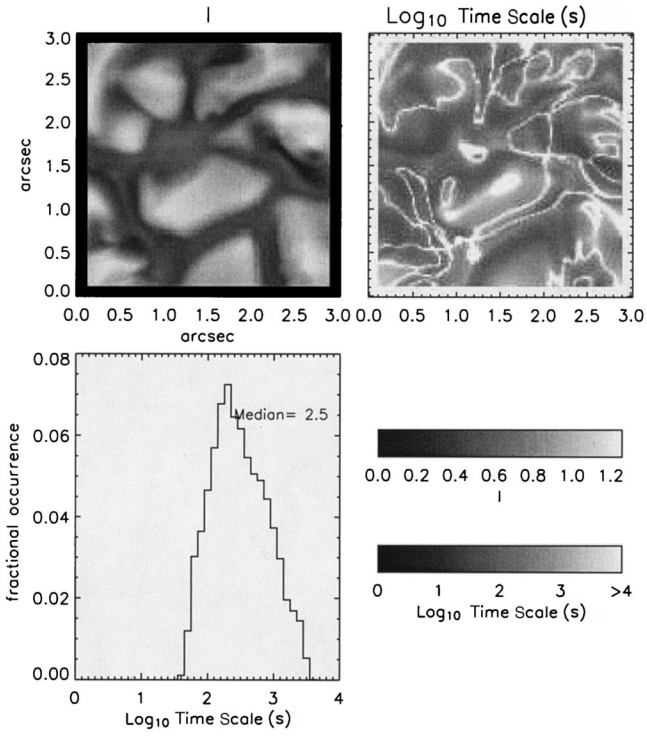

Fig. 13. Computed, convolved intensities I from the magnetoconvection simulation (top left), time scales $|I/(\mathrm{d}I/\mathrm{d}t)|$ (top right), and the distribution of time scales (bottom left). Time scales were computed from simple differences between similar data taken 30 s before and after the image shown. Only those values with significantly large values of $\mathrm{d}I/\mathrm{d}t$ were included in the time-scale plot and histogram.

$$ S_i = {S_i}^0 + \frac{\mathrm{d}S}{\mathrm{d}t}\delta t $$

so that, for a signal-to-noise ratio >3,

$$ \frac{1}{{S_i}^0}\frac{\mathrm{d}S}{\mathrm{d}t}\delta t \le \frac{1}{3}, \text{ or } \delta t \le \frac{T}{3}. $$

T is a typical time scale for surface feature evolution. With $T \approx 30$ s, we find that integration times should be a maximum of 10 s. This provides justification for our choice of integration times in Figs. 6–10. Ten seconds is a lower limit in practical terms because, as noted above, spectropolarimetry will probably be performed with pixel sizes larger than the diffraction limit, so the convolution should be done with a corresponding broader point-spread function. In passing, we note that, for some important goals to be met by solar spectropolarimetry, accurate Stokes measurements should be made not along a single slit

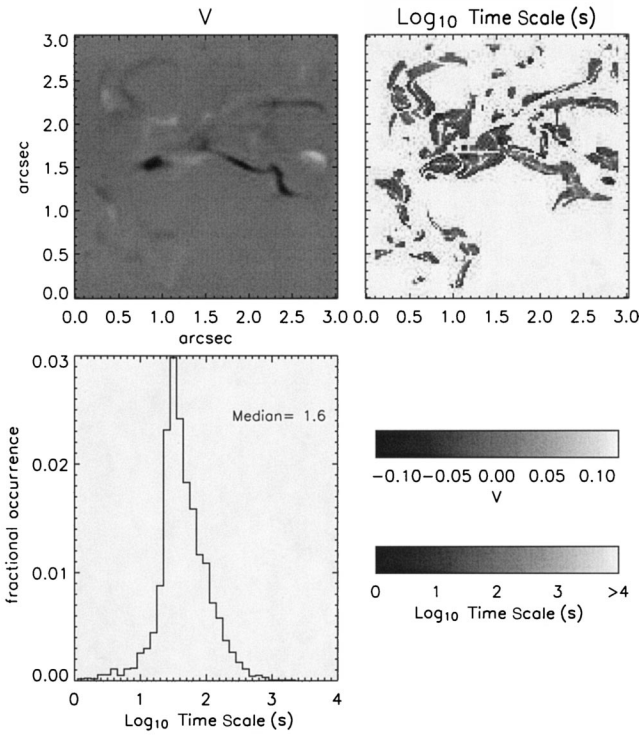

Fig. 14. Same as Fig. 13 except that data are shown for Stokes V. The same figures for Q and U are similar to those modeled for a typical region of the quiet Sun. Time scales for variation of Q, U, and V are nearly an order of magnitude smaller than those for I; and Q and U have median values of $\log_{10}$(time scales) of 1.6 and 1.5, respectively. Unlike Fig. 13, only those regions with significant values of both V and dV/dt were included in the time-scale plot and histogram.

projected onto the solar surface but within a given area, all within 10 s or so. This requirement implies the need for an image slicer or integral field unit.

4. Discussion

Our results can be summarized as follows:

- If modulation and demodulation can be done fast, say above 400 Hz, then the cross-talk issues go away [rms cross talk varies roughly with (modulation rate)$^{-1}$ at high frequencies because of the behavior of the image motion power spectra with frequency].
- Read rates of modern detectors are still too slow, $\approx$40 Hz, because the detectors are physically large. Thus cross talk remains a major issue, unless charge caching devices can be used. Such devices are being examined for the ATST and other projects.[19]
- Modulation and demodulation rates are at present unfortunately similar to the peaks in the residual power spectra of current tip–tilt correction systems, which also lie near 40 Hz. Ideally the modulation and demodulation should be done at frequencies that are at least several times this.
- Continuously rotating retarders compare reasonably well with other devices and have advantages of simplicity and large physical size—they can thus be used in relatively large beams as envisaged for ATST, for example. It is not clear that liquid crystals will be large enough or able to take the heat load for the ATST and perhaps other future instruments. Furthermore, rotating retarders can be used to measure Stokes parameters of spectral lines that differ widely in wavelength, an important capability for several science cases of interest.
- Solar evolution is an important issue when observed at high angular resolution. It limits the integration times (and hence signal-to-noise ratios) to 10 s or so. As noted by Keller,[19] unfortunately the limiting time scales decrease with increasing angular resolution as magnetic elements move faster from pixel to pixel.
- It is interesting that, although there are penalties for use of continuously rotating retarders, the computed cross-talk values for them are generally not dramatically larger (they are, at worst, just factors of several larger) than those for double liquid-crystal schemes. Thus rotating retarders should remain important modulation devices for existing and new instruments under development and construction.

We conclude, not surprisingly, that even lowest-order AO correction (just tip and tilt) is essential for accurate spectropolarimetric measurements at very high angular resolution, below 0.3 arc sec, say. If modulation can be done at say $f = 400$ Hz instead of 40 Hz, then one can take great advantage of the rapid $(1/f)$ decline of cross talk with modulation frequency, shown in Figs. 6–10. Alternatively, one can attempt to move the peak in the residual power spectrum for residual image motion to higher frequencies for the same (e.g., 40 Hz) modulation frequency by driving AO systems to the highest frequencies possible. The frequency of the peak (currently at approximately 40 Hz) in the residual image motion spectrum as well as the total power left are determined by the closed-loop servo bandwidth of the AO system. A higher bandwidth means less residual power and the peak shifts to higher frequencies. The new AO system under development at NSO's Sacramento Peak Observatory has approximately twice the bandwidth of the low-order system. It is conceivable that with more efficient AO correction systems, such as the new NSO system, slower modulation frequencies may suffice for most polarimetry applications.

The differences between the single, continuously rotating-retarder schemes and the stepped schemes are significant, but larger benefits can be expected by an increase in the modulation frequency. It seems appropriate that we place the largest efforts into determining how to modulate and read as fast as possible.

Several issues remain for future studies. One key issue that will be important for the ATST project is telescope polarization at a level $\lesssim$1% before the polarimeter.[19] The above technique could be applied to the case of seeing-induced changes in the Stokes parameters as viewed through a polarizing telescope.

This should show a clear advantage of a balanced modulation scheme. We plan to study the effects of correcting for higher-order distortions with new AO systems using the formalism applied here.

Appendix A. Typographical Corrections to the Paper of Lites

The following lists typographical errors and corrections in Lites's paper[5]:

	Original	Corrected
Eqs. (8) and (25)	$\omega_r/[\ldots]$	$1/[\ldots]$
Eq. (21)	$\exp(-\pi\nu T)$	$\exp(-i\pi\nu T)$
Last sentence of Section III.D	$\hat{H}_{ri}{}^2$	$\hat{H}_{ri}{}'^2$
Eq. (24), first term	$\exp(ix_1)$	$\exp(-ix_1)$

We thank Bob Stein and Åke Nordlund for making their numerical simulations available to us. C. U. Keller acknowledges support from the Alexander von Humboldt Foundation through the Friedrich Wilhelm Bessel research award.

References

1. E. N. Parker, *Cosmical Magnetic Fields* (Clarendon, Oxford, UK, 1979).
2. J. O. Stenflo, *Solar Magnetic Fields: Polarized Radiation Diagnostics*, Vol. 189 of the Astrophysics and Space Science Library (Kluwer Academic, Boston, Mass., 1994).
3. T. Shimizu, "Solar-B," Adv. Space Res. **29,** 2009–2015 (2002).
4. T. Rimmele, S. L. Keil, C. U. Keller, F. Hill, M. Penn, B. Goodrich, S. Hegwer, R. Hubbard, J. Oschmann, and M. Warner, "Science objectives and technical challenges of the Advanced Technology Solar Telescope," in *Current Theoretical Models and High Resolution Solar Observations: Preparing for ATST*, Vol. 286 of the Astronomical Society of the Pacific Conference Series, A. A. Pevtsov and H. Uitenbroek, eds. (Astronomical Society of the Pacific, San Francisco, Calif., 2003), pp. 3–22.
5. B. W. Lites, "Rotating waveguides as polarization modulators for Stokes polarimetry of the sun: evaluation of seeing-induced crosstalk errors," Appl. Opt. **26,** 3838–3845 (1987).
6. P. H. Seagraves and D. F. Elmore, "Use of Mueller and non-Mueller matrices to describe polarization properties of telescope-based polarimeters," in *Polarization Analysis and Measurement II*, D. H. Goldstein and D. B. Chenault, eds., Proc. SPIE **2265,** 231–238 (1994).
7. J. C. del Toro Iniesta and M. Collados, "Optimum modulation and demodulation matrices for solar polarimetry," Appl. Opt. **39,** 1637–1642 (2000).
8. C. U. Keller, "Instrumentation for astrophysical spectropolarimetry," in *Astrophysical Spectropolarimetry*, J. Trujillo-Bueno, F. Moreno-Insertis, and F. Sánchez, eds. (Cambridge U. Press, Cambridge, UK, 2002), pp. 303–354.
9. J. O. Stenflo and H. Povel, "Astronomical polarimeter with 2-D detector arrays," Appl. Opt. **24,** 3893–3898 (1985).
10. C. U. Keller, F. L. Deubner, U. Egger, B. Fleck, and H. P. Povel, "On the strength of solar intra-network fields," Astron. Astrophys. **286,** 626–634 (1994).
11. A. M. Gandorfer and H. P. Povel, "First observations with a new imaging polarimeter," Astron. Astrophys. **328,** 381–389 (1997).
12. F. Roddier, *Adaptive Optics in Astronomy* (Cambridge U. Press, Cambridge, UK, 1999).
13. G. B. Scharmer, K. Bjelksjo, T. K. Korhonen, B. Lindberg, and B. Petterson, "The 1-meter Swedish solar telescope," in *Innovative Telescopes and Instrumentation for Solar Astrophysics*, S. L. Keil and S. V. Avakyan, eds., Proc. SPIE **4853,** 341–350 (2003).
14. J. Sánchez Almeida, "Modulation scheme for the polarimeter for the SST," Tech. Rep. (Instituto Astrofysicas Canarias, La Laguna, Tenerife, 1994).
15. D. F. Elmore, B. W. Lites, S. Tomczyk, A. P. Skumanich, R. B. Dunn, J. A. Scheunke, K. V. Streander, T. W. Leach, C. W. Chambellan, H. K. Hull, and L. B. Lacey, "The Advanced Stokes Polarimeter: a new instrument for solar magnetic field research," in *Polarization Analysis and Measurement*, D. H. Goldstein and R. A. Chipman, eds., Proc. SPIE **1746,** 22–33 (1992).
16. V. Martínez Pillet, M. Collados, J. Sánchez Almeida, V. González, A. Cruz-Lopéz, A. Manescau, E. Joven, E. Paez, J. J. Díaz, O. Feeney, V. Sánchez, G. Scharmer, and D. Soltau, "LPSP and TIP: full Stokes polarimeters for the Canary Islands observatories," in *High Resolution Solar Physics: Theory, Observations and Techniques*, Vol. 184 of the Astronomical Society of the Pacific Conference Series, T. Rimmele, R. Raddick, and K. S. Balasubramaniam, eds. (Astronomical Society of the Pacific, San Francisco, Calif., 1999), pp. 264–272.
17. C. U. Keller, J. W. Harvey, and M. S. Giampapa, "SOLIS: an innovative suite of synoptic instruments," in *Innovative Telescopes and Instrumentation for Solar Astrophysics*, S. L. Keil and S. V. Avakyan, eds., Proc. SPIE **4853,** 194–204 (2003).
18. K. Sankarasubramanian, D. F. Elmore, B. W. Lites, M. Sigwarth, T. R. Rimmele, S. L. Hegwer, S. Gregory, K. V. Streander, L. M. Wilkins, K. Richards, and C. Berst, "Diffraction limited spectro-polarimeter—phase I," in *Polarimetry in Astronomy*, S. Fineschi, ed., Proc. SPIE **4843,** 414–424 (2003).
19. C. U. Keller, "Polarimetry with the ATST," in *Current Theoretical Models and High Resolution Solar Observations: Preparing for ATST*, Vol. 286 of the Astronomical Society of the Pacific Conference Series, A. A. Pevtsov and H. Uitenbroek, eds. (Astronomical Society of the Pacific, San Francisco, Calif., 2003), pp. 31–44.
20. G. B. Scharmer, B. V. Gudiksen, D. Kiselman, M. G. Löfdahl, and L. H. M. R. van der Voort, "Dark cores in sunspot penumbral filaments," Nature (London) **420,** 151–153 (2002).
21. R. F. Stein and Å. Nordlund, "Solar surface magneto-convection and dynamo action," in *SOLMAG 2002: Proceedings of the Magnetic Coupling of the Solar Atmosphere Euroconference*, ESA SP-505, H. Saway-Lacoste, ed. (European Space Agency, Noordwijk, The Netherlands, 2002), pp. 83–89.